

Use of endogenous NADH fluorescence for real-time in situ visualization of epicardial radiofrequency ablation lesions and gaps

Marco Mercader,¹ Luther Swift,² Sumit Sood,² Huda Asfour,³ Matthew Kay,^{2,3} and Narine Sarvazyan^{1,2}

¹The George Washington University Medical Faculty Associates, Division of Cardiology, Washington; ³Department of Electrical and Computer Engineering, The George Washington University, Washington; and ²Department of Pharmacology & Physiology, The George Washington University Medical Center, Washington, District of Columbia

Submitted 7 December 2011; accepted in final form 5 March 2012

Mercader M, Swift L, Sood S, Asfour H, Kay M, Sarvazyan N. Use of endogenous NADH fluorescence for real-time in situ visualization of epicardial radiofrequency ablation lesions and gaps. *Am J Physiol Heart Circ Physiol* 302: H2131–H2138, 2012. First published March 9, 2012; doi:10.1152/ajpheart.01141.2011.—Radiofrequency ablation (RFA) aims to produce lesions that interrupt reentrant circuits or block the spread of electrical activation from sites of abnormal activity. Today, there are limited means for real-time visualization of cardiac muscle tissue injury during RFA procedures. We hypothesized that the fluorescence of endogenous NADH could be used as a marker of cardiac muscle injury during epicardial RFA procedures. Studies were conducted in blood-free and blood-perfused hearts from healthy adult Sprague-Dawley rats and New Zealand rabbits. Radiofrequency was applied to the epicardial surface of the heart using a 4-mm standard blazer ablation catheter. A dual camera optical mapping system was used to monitor NADH fluorescence upon ultraviolet illumination of the epicardial surface and to record optical action potentials using the voltage-sensitive probe RH237. Epicardial lesions were seen as areas of low NADH fluorescence. The lesions appeared immediately after ablation and remained stable for several hours. Real-time monitoring of NADH fluorescence allowed visualization of viable tissue between the RFA lesions. Dual recordings of NADH and epicardial electrical activity linked the gaps between lesions to postablation reentries. We found that the fluorescence of endogenous NADH aids the visualization of injured epicardial tissue caused by RFA. This was true for both blood-free and blood-perfused preparations. Gaps between NADH-negative regions revealed unablated tissue, which may promote postablation reentry or provide pathways for the conduction of abnormal electrical activity.

catheter ablation; arrhythmias; lesion; imaging; atrial fibrillation

RADIOFREQUENCY ABLATION (RFA) is an effective therapy for treating atrial and ventricular rhythm disturbances (16). Nearly 100,000 RFA procedures are performed annually in the United States to treat cardiac arrhythmias (29). RFA targets the key elements of reentrant pathways and/or abnormal ectopic loci without damaging a significant amount of adjacent healthy myocardium and coronary vessels.

RFA lesion size is not simply a function of delivered energy but depends on many factors, including the contact between the catheter tip and the tissue, the thickness of the myocardium, the amount of blood flow, and the presence of fat (16, 33). Conventional electroanatomical mapping systems map mainly the location of the catheter tip but not the extent of tissue injury caused by ablation. Therefore, as of today, RFA ablation

lesions are created with minimal information regarding the physiological condition of the affected tissue.

Gaps of excitable tissue between ablation lesions are directly related to arrhythmia recurrences. Two main strategies have been proposed to reduce the incidence of gaps. The first is to improve ablation devices, which includes the development of multipolar and linear catheters (3, 15), balloon-based technologies using lasers, focused ultrasound and cryoinjury (9, 26), as well as pressure sensor-equipped catheters (34). The second strategy is to visualize RFA lesions during the ablation procedure (1, 7, 10–12, 20, 31). Such visualization could be based upon acute changes in the chemical and/or physical properties of the damaged tissue. The approach described in this article is based upon imaging the fluorescence of endogenous NADH (fNADH) using low-intensity ultraviolet (UV) light illumination.

NADH is a coenzyme that is present within all intact cells. Once NADH is released from the mitochondria of damaged cells and/or converted to its oxidized form, its fluorescence markedly declines. Recent advances in tumor surgery have used endogenous fNADH as a means to monitor tissue necrosis during RFA surgery and provided general proof of the method's feasibility (21, 22). To the best of our knowledge, this is the first imaging of fNADH as a means to visualize viability of cardiac tissue during RFA procedures. Our results show that reductions in epicardial fNADH caused by RFA are so substantial that the method reveals lesions not only in blood-free but also in blood-perfused cardiac preparations.

METHODS

Animal procedures. Ex vivo experiments were conducted using Sprague-Dawley (200–300 g) and New Zealand White rabbits (2.5–3.5 kg). Animals were heparinized and anesthetized using standard procedures (2, 17). Hearts were excised, and the aorta was cannulated and Langendorff-perfused at constant pressure (50 mmHg) with oxygenated, buffered Tyrode solution at room temperature. During the ablation period, hearts were placed on top of a grounding pad and submerged in 37°C Tyrode solution.

In situ experiments were performed using anesthetized open-chest rats (200–300 g Sprague-Dawley). After an intraperitoneal injection of Telazol (40 mg/kg), the hair on the chest and back was shaved, the animal was immobilized on a heated platform, and an ablation pad was placed beneath the animal. Immediately after opening the chest cavity, ablations were carried out as the exposed epicardial surface was imaged. All anesthesia and euthanasia procedures were approved by the George Washington University Medical Center Institutional Animal Care and Use Committee.

Ablation protocols and NADH recordings. Radiofrequency energy was delivered using a noncooled blazer catheter with a 4-mm tip (EP Technologies, Boston Scientific). Tip temperatures ranged between 50 to 70°C. The catheter was placed perpendicular to the epicardial

Address for reprint requests and other correspondence: N. Sarvazyan, Pharmacology and Physiology Dept., The George Washington Univ., 2300 Eye St., Washington DC 20037 (e-mail: phynas@gmail.com).

surface. Ablation durations varied from 15 to 60 s with a maximum power of 50 watts. The epicardial surface was illuminated with UV light (350/25 nm) using a 100-watt mercury lamp (Zeiss HBO100 W/2). To record the epicardial fluorescence of NADH, the emitted light was filtered (460/25 nm) and imaged using a charge-coupled device camera (Andor Ixon DV860) that has high quantum efficiency for wavelengths corresponding to NADH fluorescence (80% quantum efficiency at 460 nm).

Optical mapping experiments. Hearts were stained with the potentiometric dye RH237 (10 μ M final concentration; Molecular Probes). To reduce motion artifact, blebbistatin was added to the perfusate at a final concentration of 10 μ M. A dual optical mapping system comprised of two cameras (Andor IXON DV860s) fitted with a dual port adapter (Andor CSU Adapter Dual Cam) and a dichroic mirror (610 nm) was used to image the epicardial fluorescence of RH237 [250–500 frames/s (fps)] and NADH (2 fps) from the same field of view (32). To record optical action potentials, the epicardium was illuminated using two light-emitting diodes (LumiLEDs, 530/35 nm). The resulting RH237 fluorescence was long pass filtered at 680 nm. NADH fluorescence was recorded with the other camera as described above. The fluorescence of RH237 was processed to subtract background fluorescence from each image, and signals for each pixel were normalized. RH237 fluorescence signals were smoothed using a median temporal filter (3 sample width). Isochronal maps of activation times were generated to show wave front propagation. The average amplitude of optical action potentials at each pixel was computed to reveal spatial changes in the amount of electrically active tissue.

Triphenyltetrazolium chloride staining. Triphenyltetrazolium chloride (TTC) vital staining is a standard procedure for assessing acute necrosis. It relies on the ability of dehydrogenase enzymes and NADH

to react with tetrazolium salts to form a formazan pigment. Immediately after the imaging protocol, the tissue was retrograde-perfused with Tyrode solution containing 1.0% TTC. Afterward, the heart was submerged in the TTC solution for an additional 8 min. Metabolically active tissue appeared crimson. Necrotic tissue appeared white.

RESULTS

Appearance of RFA lesions in excised, blood-free rat and rabbit hearts. In total, 16 lesions in 8 rat hearts and 8 lesions in 3 rabbit hearts were studied. When observed on the NADH-sensitive channel, ablated areas appeared markedly dark when compared with the surrounding myocardium (Fig. 1A, center). TTC staining revealed areas of irreversible injury consistent with the shape and the size of RFA lesions (Fig. 1A, right). During the 1- to 2-h experiments, fNADH levels in ablated tissue did not return to their preablation values, and the size of the lesions did not change significantly ($n = 3$; Fig. 1B, row on top). Over time, lesion borders became more homogenous ($n = 3$; Fig. 1C). A systematic comparison of fNADH lesions with TTC-negative areas showed that lesion size and shape matched with better than 95% accuracy (Fig. 2).

Identification of functional gaps between RFA lesions. To study propagation through interlesion isthmuses, we optically mapped wavefronts of electrical activity between two closely placed RFA lesions ($n = 5$). Hearts were stained with RH237 and then ablated at two adjacent sites on the left ventricular epicardium. A bipolar pacing electrode was placed on the

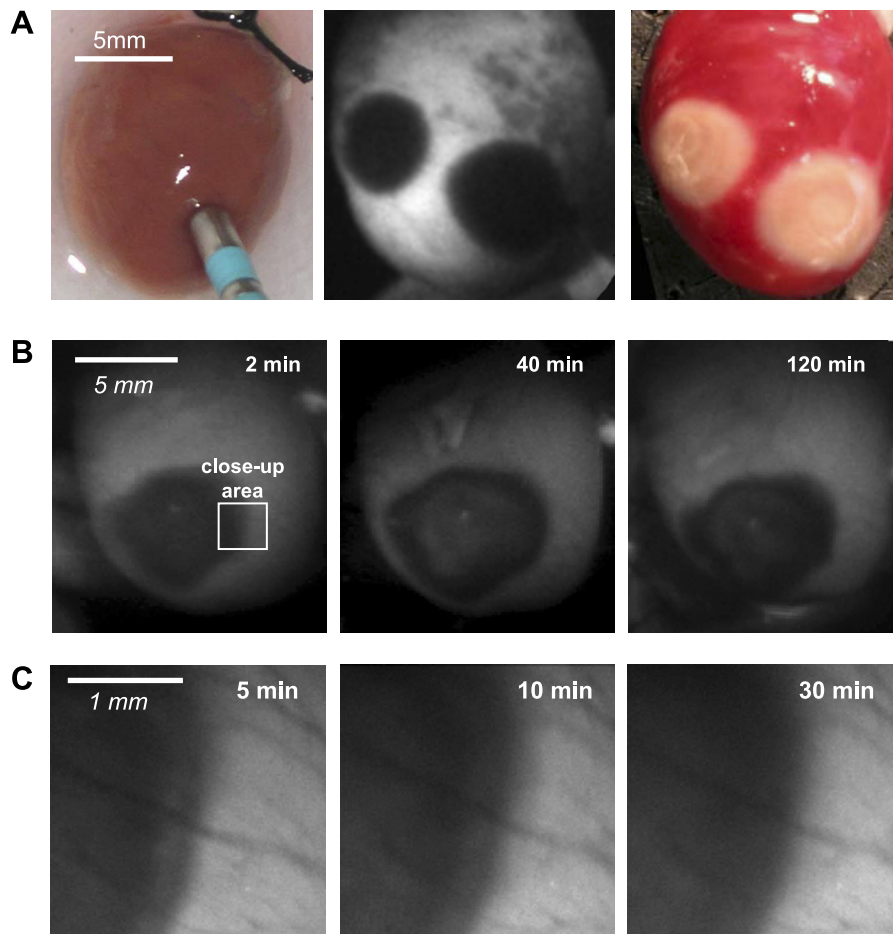


Fig. 1. Radiofrequency ablation (RFA) lesions in blood-free excised rat hearts. *A*: a radiofrequency (RF) catheter in the position to deliver energy onto the epicardial surface of a rat heart, followed by appearance of two dark RFA lesions as revealed by fluorescent NADH (fNADH) imaging. The image on the right illustrates appearance of the same two RFA lesions after triphenyltetrazolium chloride (TTC) staining. Metabolically active tissue appears red, and irreversibly damaged tissue shows as white. *B*: three sequential snapshots of epicardial fNADH at different time points after ablation using low-magnification settings. *C*: as time progressed, fNADH lesion borders became more homogenous. This is illustrated by high-magnification snapshots of the lesion shown in *B* at intermediate time points.

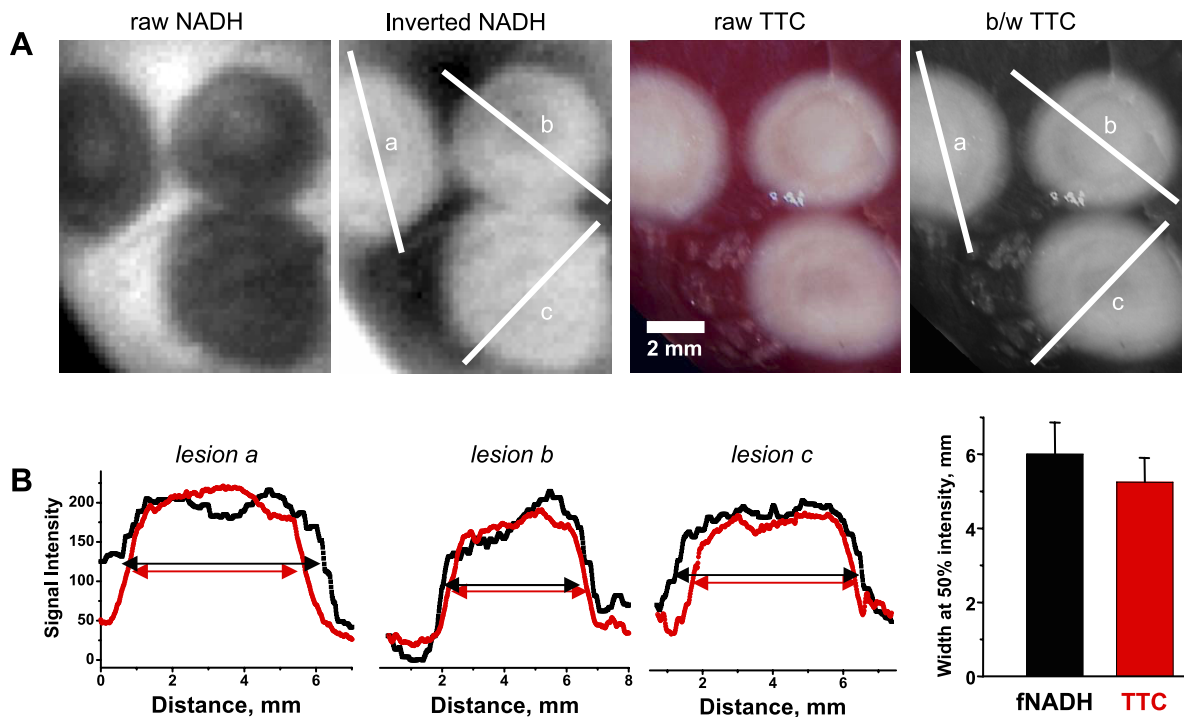


Fig. 2. Quantitative comparison between sizes of fNADH lesions and their respective TTC staining. A: three RFA lesions on the surface of a rabbit heart. For direct visual and pixel profile comparison, gray scale of fNADH images was inverted to show previously dark lesions in white, whereas the color TTC images were converted to black and white (b/w). Intensity profiles across each lesion were then compared. The three graphs in B correspond to the intensity profile through each lesion. The bar graph shows that widths of the lesions were not significantly different when examined using fNADH and TTC staining.

epicardium above the RFA lesions, and current was applied at two times the diastolic threshold. An example of spontaneous reentrant circuits around the lesions when a functional isthmus was present is illustrated in Fig. 3. It shows 1) an overlay of epicardial fNADH with an isochronal activation map, 2) optical action potentials, and 3) sequential RH237 images. The full sequence can be seen as an online supplemental movie (The online version of this article contains supplemental material.).

To create the isochronal maps shown in Fig. 3A, optical action potentials were normalized to show propagating wavefronts in an all-or-none fashion. Normalization is useful for illustrating propagation but obscures the true optical action potential amplitudes. To better represent true optical action potential amplitudes, the RH237 signal at each pixel was scaled as a percentage of the maximum optical action potential amplitude for all the pixels. The interlesion profile of the optical action potential amplitude is shown in Fig. 4A as an $x-t$ plot for five sequential beats, with the x -axis being the distance between the centers of the two lesions. The interlesion profile of action potential amplitude was then compared with the interlesion profile of fNADH intensity (Fig. 4B). The two were highly correlated (Fig. 4, B and C). These findings suggest that fNADH loss can serve as an endogenous live marker for the diminished functional state of the tissue at the ablation site.

Appearance of RFA lesions on RH237-sensitive channel. The epicardial fluorescence of RH237 faded due to washout of the dye (Fig. 5A). However, in ablated tissue, the fluorescence of RH237 declined much slower (Fig. 5B) than in unablated tissue (Fig. 5B). Over time, the background RH237 fluorescence of the lesions was brighter than that of unablated tissue (Fig. 5A, right). The size of these “RH237 lesions” was

significantly smaller (by $19 \pm 5\%$, $P < 0.001$, $n = 7$) than corresponding dark “fNADH lesions” (Fig. 5C). This matched with the internal ring-like structures sometimes seen on both fNADH and TTC images (Fig. 2A). We believe that RH237 lesions result from acute damage to epicardial capillaries. This may occur at the site of direct resistive heating immediately beneath the electrode and impede the washout of RH237. We further suggest that, by comparing two types of lesions (fNADH vs. fRH237), one can distinguish areas of resistive heating from conductive heat transfer (Fig. 5D).

Visualization of RFA lesions in blood-perfused rat hearts. To show the feasibility of fNADH-based imaging in blood-perfused animals, ablation was performed immediately after opening the chest. fNADH images were acquired in the same way as in the excised heart experiments. Major blood vessels appeared as dark tracks within these images. Even so, RFA lesions were clearly evident, indicating that cardiac muscle with its dense supply of mitochondria provides enough fNADH to reveal the unablated tissue that borders a lesion (Fig. 6A). fNADH images became dark when the epicardial surface of the heart was submerged in blood (Fig. 6B). When blood was displaced from the epicardial surface using a sheet of transparent polyvinylidene chloride, RFA lesions were clearly seen. The data shown in Fig. 6 are representative of four experiments.

DISCUSSION

As of today, RFAs are performed with minimal real-time information regarding the physiological state of the ablated tissue. Limited assessments include electrogram amplitude, the

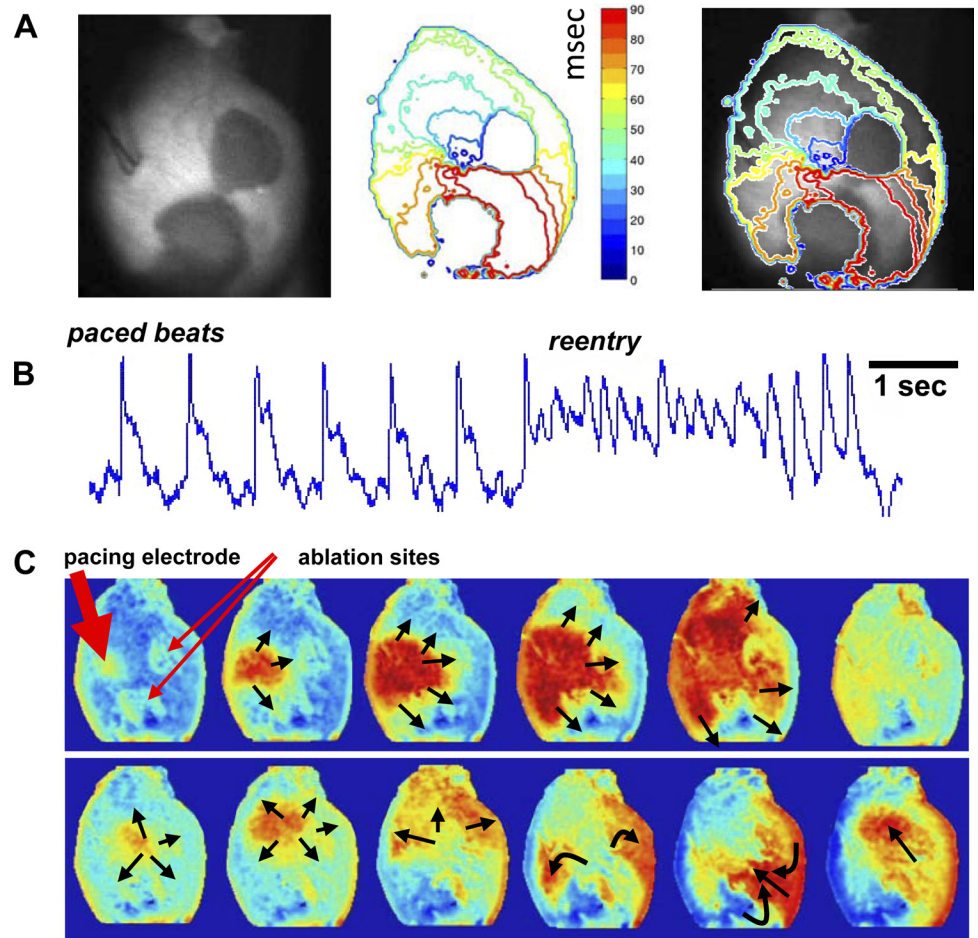


Fig. 3. Dual imaging of epicardial electrical activity and fNADH: propagation through narrow isthmus between two RFA lesions. *A*: two fNADH lesions are shown in *left*. The corresponding isochronal map of electrical activity recorded using the voltage-sensitive dye RH237 is shown in the *center*. The two were overlaid in the *right*. *B*: pseudo electrocardiogram (ECG) trace reconstructed by averaging optical action potentials from all pixels in individual frames. It corresponds to the sequence shown in *C* and the corresponding supplemental movie. *C*: sequential snapshots of processed RH237 sequence that illustrate propagation of paced beats and reentry around the two lesions. The red arrows point to the location of a pacing electrode and RF ablation sites. Black arrows indicate the direction of propagating wavefronts. A supplementary movie corresponding to this figure is provided online.

ability to pace and capture ablated tissue, and maneuvers to pace and detect gaps in linear lesions created by multipoint ablations (23). Yet, these assessments provide only limited information regarding the extent and physiological state of the lesion. Second, it is very difficult to determine whether electrical isolation results from acute irreversible muscle damage, functional changes in reversibly injured cells, or from temporary edema. In the case of edema, it may subside after a few weeks, potentially restoring abnormal electrical conduction. The advantage of fNADH imaging is that it reveals irreversible muscle damage without contrast agents, tracers, or dyes. Because NADH is predominantly localized to the mitochondria, fNADH imaging should be insensitive to edema because the interstitial fluid concentration of NADH is negligible. From a clinical perspective, the fact that fNADH lesions are stable for >1 h (Fig. 1*B*) suggests that lesions could be examined or reexamined at almost any time during an ablation procedure.

The final size of an RF lesion is dependent upon the magnitude and duration of the applied energy. Our ablation parameters produced lesions having an average diameter of 5 mm, similar to those created in the clinic. Our imaging system provided images that revealed interlesion gaps as small as 0.5 mm (see Fig. 2). Smaller lesions could be revealed using higher-magnification lenses or a camera with higher spatial resolution.

Abundant mitochondria make cardiac myocytes particularly suitable for fNADH imaging. Reduced fNADH at the site of

the RFA lesions indicates a loss of myocyte membrane integrity, since cell and mitochondrial membranes are rapidly damaged by thermal stress. Notably, cardiac muscle cell necrosis within the ablation site does not necessarily mean that the integrity of all underlying structures, such as coronary vessels, is destroyed. In our experiments, we did not observe the disruption of major coronary vessel structure. This is because, if vessels were disrupted, then tissue downstream of damaged vessels would become ischemic, causing fNADH to increase (17). Yet, fNADH levels near the lesions did not change significantly before and after ablation. Other evidence of intact coronary structure was the homogeneity of postablation TTC staining: any major vessel damage would have been indicated as areas of unstained tissue outside the RFA lesion. However, all RFA lesions stained with TTC were localized strictly to the RF lesion site (Figs. 1 and 2). Finally, observation of intact vessels on the epicardial surface did not indicate severe damage to major vessels at the ablation sites.

One may perceive a contradiction between the reported increase in fNADH during ischemic injury (17) and fNADH decrease upon thermal damage. This apparent contradiction is explained as follows. About 30% of cardiomyocyte volume is comprised of mitochondria that contain a large amount of NADH. Because of this, changes in the level of fNADH from myocytes can be measured with relative ease. When the sarcolemma and mitochondrial membranes are disrupted by heat, NADH is lost, and fNADH levels immediately fall. During

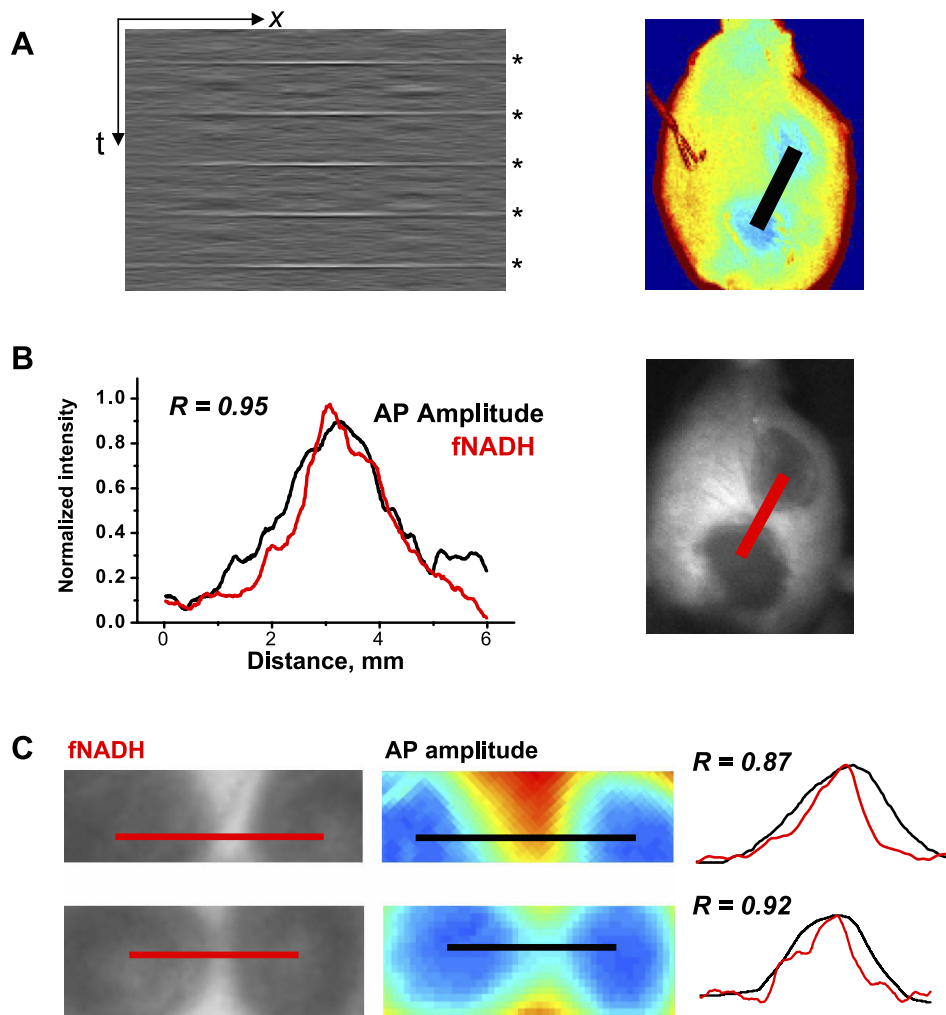


Fig. 4. fNADH and electrical activity across the isthmus between two RFA lesions. **A:** the gray box is an x - t representation of the amplitudes of five sequential action potentials along the black line in the adjacent pseudocolored image. The latter shows the amplitudes of action potentials derived from RH237 data. The x -axis is the distance between the two lesions. The y -axis represents time with action potentials indicated by asterisks on the *right*. **B:** the graph shows interlesion intensity profile for fNADH (red line) with the profile of the action potential (AP) amplitude (black line). The two profiles had Pearson's correlation coefficient of $r = 0.95$, $P < 0.001$. **C:** closeup of two other interlesion gaps. Image on the *left* shows interlesional gap as seen on fNADH channel. The corresponding image on the *right* is a pseudocolored representation of action potential amplitudes computed from RH237 data. The graph shows normalized intensity profiles for fNADH and action potential amplitudes from corresponding red and black lines. The numbers stands for Pearson's correlation coefficient values.

hypoxia and/or ischemia, cellular integrity is preserved, but oxygen availability is reduced. Oxygen serves as a final electron acceptor in the mitochondrial electron chain, and its decline leads to NADH accumulation (5). Thus, ischemia causes an increase in fNADH in a time-dependent manner (24, 32). For example, if coronary perfusion is disrupted before the ablation, patches of ischemic tissue with elevated fNADH levels may be observed adjacent to the darker circular fNADH lesions. Therefore, one concludes that acute tissue ischemia is, in fact, helpful in visualizing RFA lesions via fNADH due to increased contrast between the lesion and the surrounding tissue. A situation involving a healed myocardial infarction is different. Scar contains a significant amount of collagen and as such can contribute to background fluorescence in a spectral range similar to fNADH. Choosing more selective filters and/or the use of ratiometric approaches should be able to distinguish the two, but additional experiments are required to validate these predictions.

As mentioned earlier, one of the main advantages of monitoring endogenous fNADH is that it can be done without additional probes or contrast agents. Because changes in fluorescence reflect acute biochemical changes, lesions are seen almost immediately. Imaging modalities such as magnetic resonance imaging (MRI) (8, 20), C-arm computed tomogra-

phy (CT) (12), and contrast echocardiography (18) are excellent tools in detecting parameters resulting from heat-induced biophysical changes. However, contrast agents are required to visualize changes in real time. Although MRI and C-arm CT provide high spatial resolution, it could take up to 30 min to visualize cell necrosis. Echocardiography is faster but suffers from low spatial resolution and limited field of view. Other modalities based on physical tissue changes, including alteration in tissue elasticity, impedance, or absorption, have also been explored (1, 7, 10, 31). While such strategies provide real-time feedback and may predict lesion size and depth, they also require significant data processing and do not provide direct visualization of the ablated region.

Today a majority of RFA procedures are endocardial, but ~ 10 – 20% are epicardial (4, 6, 13, 30). Epicardial substrates are frequently observed for VT, including $>20\%$ of postinfarct VTs and $>30\%$ of VTs from nonischemic cardiomyopathy, particularly for Chagas disease (14, 30). RFA of these epicardial substrates may use a percutaneous approach that involves the subxiphoid placement of sheaths into an intact, closed pericardial space (30). fNADH imaging seems to be particularly feasible for these procedures. Conventional endoscopes equipped with UV-compatible optics and image capture devices would be suitable for this purpose. Air insufflation

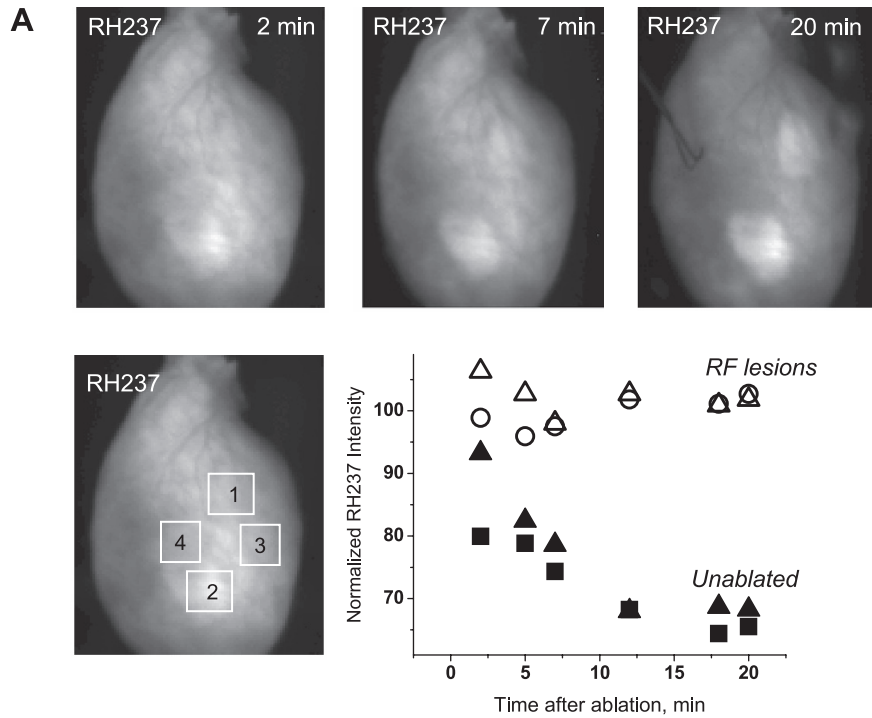
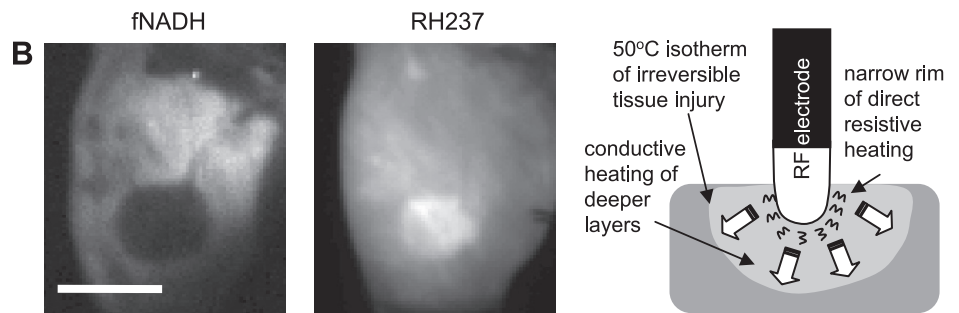


Fig. 5. Retention of voltage-sensitive dye within RFA lesions. *A*: excised rat heart was stained with RH237 and ablated at two sites. Images on *top* illustrate temporal changes in epicardial RH237 fluorescence. The solid points, which trend downward over time, correspond to regions of interest (ROIs) in unablated areas. The open points, which remain stable over time, correspond to ROIs in the lesion areas. *B*: *left*, representative case of RFA lesion appearance on fNADH and RH237 channels with fNADH lesion being noticeably larger. Bar = 5 mm. *Right*, schematic representation of lesion formation by radiofrequency catheter. Temperatures above 50°C cause irreversible myocardial injury; at temperatures above 100°C, boiling occurs at the electrode-tissue contact, forming a coagulum.



through the endoscope could be used to expand the pericardial space for adequate visualization of ablation sites. In a clinical setting, insufflation with carbon dioxide rather than air would likely reduce the risk of air embolization (25). Most importantly, our findings shown in Fig. 6 show the feasibility of fNADH imaging for endocardial procedures. The latter is possible if blood is displaced in front of an endoscope, either by inflatable balloons (9, 19) or via carbon dioxide insufflation mentioned earlier.

Additional studies are required to determine whether fNADH imaging could be used to visualize RFA lesions in the atria, i.e., for the treatment of atrial fibrillation. Trabeculation, the intricate geometry of pulmonary veins, the presence of collagen layers, and other structural heterogeneities make fNADH-based visualization of atrial RFA lesions more complex compared with epicardial lesions.

The method described in this manuscript is a simple, straightforward way to monitor acute myocardial damage while performing RFA. If implemented clinically, it has the

potential to shorten the time and improve the efficiency of ablations, minimize unnecessary tissue injury that may cause post-RFA complications, and decrease postablation recurrence of arrhythmias. fNADH imaging may also be useful for mechanistic studies of tissue injury near the RFA sites (28) and for assessment of drugs that may alter electrical propagation between interlesion gaps (27). We also believe that NADH fluorescence could be potentially very useful in identifying the ablation gaps seen after pulmonary vein isolation procedures. Last, loss of NADH fluorescence should occur regardless of energy source that leads to tissue necrosis, making this approach applicable to visualization of cryo or laser-based catheter lesions.

This study has several limitations. The feasibility of the technique was demonstrated using open-chest small animal models and not in more clinically relevant large animal models using percutaneous epicardial access; the feasibility of the technique was demonstrated only for epicardial lesions and not for endocardial lesions; and the method is limited to the

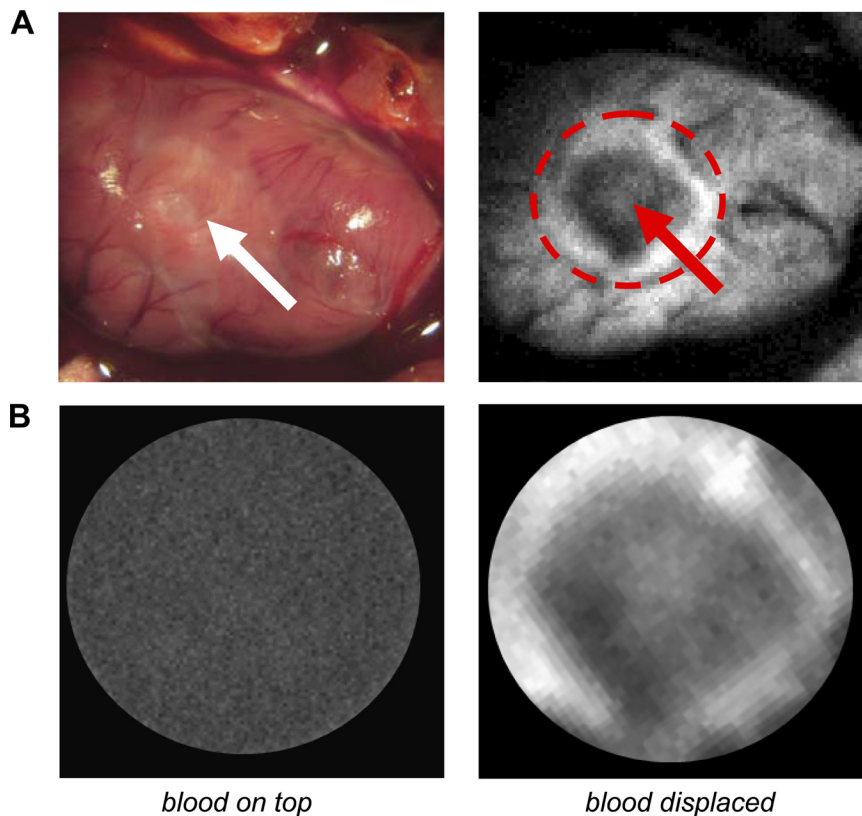


Fig. 6. RFA lesions in blood-perfused open-chest animals. Naked eye appearance of ablated heart is shown on the *left*, and the same heart appearance on fNADH channel is on the *right*. White arrows point to the center of the lesion. A: submerging the above ablated heart in externally added blood completely obscures the lesion (*left*). Displacing external blood from the heart surface using a transparent polyvinylidene chloride film camera reveals the lesion (*right*).

visualization of the surface injury. Electrically active gaps present below the epicardial surface can be missed by this technique.

In conclusion 1) RFA lesions in both blood-free and blood-perfused rat and rabbit hearts can be visualized by imaging endogenous NADH fluorescence, 2) optical action potentials can be imaged simultaneously with the endogenous fluorescence of NADH to study changes in electrical activity and tissue viability around ablation lesions and interlesion gaps, and 3) the data suggest that fNADH imaging could be employed during clinical RFA procedures via dual UV excitation/emission fiber-optic waveguide located inside a balloon catheter. Such a waveguide system could interface with a three-dimensional mapping system to provide a detailed map of cardiac muscle viability near the catheter.

GRANTS

Financial support from the George Washington Medical Faculty Associates Collaborative Research Program and the National Heart, Lung, and Blood Institute (HL-095828) is gratefully acknowledged.

DISCLOSURES

A provisional patent describing the use of NADH imaging for cardiac RF catheters was filed by the George Washington University Technology Transfer Office (#61/537,798).

AUTHOR CONTRIBUTIONS

Author contributions: M.M., M.W.K., and N.S. conception and design of research; M.M., L.M.S., S.S., H.A., M.W.K., and N.S. performed experiments; M.M., M.W.K., and N.S. interpreted results of experiments; M.M., H.A., M.W.K., and N.S. drafted manuscript; M.M., L.M.S., S.S., H.A., M.W.K., and N.S. approved final version of manuscript; H.A., M.W.K., and N.S. analyzed data; M.W.K. and N.S. edited and revised manuscript; N.S. prepared figures.

REFERENCES

- Anderson CD, Lin WC, Buttemere CR, Washington MK, Mahadevan-Jansen A, Pierce J, Nicoud IB, Pinson CW, Chari RS. Real-time spectroscopic assessment of thermal damage: implications for radiofrequency ablation. *J Gastrointest Surg* 8: 660–669, 2004.
- Asfour H, Swift LM, Sarvazyan N, Doroslovacki M, Kay MW. Signal decomposition of transmembrane voltage-sensitive dye fluorescence using a multiresolution wavelet analysis *IEEE Trans. Biomed Eng* 58: 2083–2093, 2011.
- Boersma LV, Wijffels MC, Oral H, Wever EF, Morady F. Pulmonary vein isolation by duty-cycled bipolar and unipolar radiofrequency energy with a multielectrode ablation catheter. *Heart Rhythm* 5: 1635–1642, 2008.
- Buch E, Shivkumar K. Epicardial catheter ablation of atrial fibrillation. *Minerva Med* 100: 151–157, 2009.
- Chance B, Thorell B. Fluorescence measurements of mitochondrial pyridine nucleotide in aerobiosis and anaerobiosis. 184: 931–934, 1959.
- d'Avila A. Epicardial catheter ablation of ventricular tachycardia. *Heart Rhythm* 5: S73–S75, 2008.
- Demos SG, Sharareh S. Real time assessment of RF cardiac tissue ablation with optical spectroscopy. *Opt Express* 16: 15286–15296, 2008.
- Dickfeld T, Kato R, Zviman M, Lai S, Meininger G, Lardo AC, Roguin A, Blumke D, Berger R, Calkins H, Halperin H. Characterization of Radiofrequency Ablation Lesions With Gadolinium-Enhanced Cardiovascular Magnetic Resonance Imaging. *J Am Coll Cardiol* 47: 370–378, 2006.
- Dukkipati SR, Neuzil P, Skoda J, Petru J, d'Avila A, Doshi SK, Reddy VY. Visual balloon-guided point-by-point ablation: reliable, reproducible, and persistent pulmonary vein isolation. *Circ Arrhythm Electrophysiol* 3: 266–273, 2010.
- Dumas Iii JH, Himel Iv HD, Kiser AC, Quint SR, Knisley SB. Myocardial electrical impedance as a predictor of the quality of RF-induced linear lesions. *Physiol Meas* 29: 1195–1207, 2008.
- Fleming CP, Quan KJ, Rollins AM. Toward guidance of epicardial cardiac radiofrequency ablation therapy using optical coherence tomography (Abstract). *J Biomed Opt* 15: 041510, 2010.

12. Girard EE, Al-Ahmad A, Rosenberg J, Luong R, Moore T, Lauritsch G, Boese J, Fahrig R. Contrast-enhanced C-arm CT evaluation of radiofrequency ablation lesions in the left ventricle. *JACC Cardiovasc Imaging* 4: 259–268, 2011.
13. Grimard C, Lacotte J, Hidden-Lucet F, Duthoit G, Gallais Y, Frank R. Percutaneous epicardial radiofrequency ablation of ventricular arrhythmias after failure of endocardial approach: a 9-year experience. *J Cardiovasc Electrophysiol* 21: 56–61, 2010.
14. Henz BD, do Nascimento TA, Dietrich Cde O, Dalegrave C, Hernandes V, Mesas CE, Leite LR, Cirenza C, Asirvatham SJ, de Paola AA. Simultaneous epicardial and endocardial substrate mapping and radiofrequency catheter ablation as first-line treatment for ventricular tachycardia and frequent ICD shocks in chronic chagasic cardiomyopathy. *J Interv Card Electrophysiol* 26: 195–205, 2009.
15. Himel HD, 4th Dumas JH, 3rd Kiser AC, Knisley SB. Translesion stimulus-excitation delay indicates quality of linear lesions produced by radiofrequency ablation in rabbit hearts. *Physiol Meas* 28: 611–623, 2007.
16. Huang SKS, Wood MA. *Catheter Ablation of Cardiac Arrhythmias*. Philadelphia, PA: Saunders Elsevier, 2006.
17. Kay M, Swift L, Martell B, Arutunyan A, Sarvazyan N. Locations of ectopic beats coincide with spatial gradients of NADH in a regional model of low-flow reperfusion *Am J Physiol Heart Circ Physiol* 294: H2400–H2405, 2008.
18. Khoury DS, Rao L, Ding C, Sun H, Youker KA, Panescu D, Nagueh SF. Localizing and quantifying ablation lesions in the left ventricle by myocardial contrast echocardiography *J. Cardiovasc Electrophysiol* 15: 1078–1087, 2004.
19. Kim DH, Lu N, Ghaffari R, Kim YS, Lee SP, Xu L, Wu J, Kim RH, Song J, Liu Z, Viventi J, de Graff B, Elolampi B, Mansour M, Slepian MJ, Hwang S, Moss JD, Won SM, Huang Y, Litt B, Rogers JA. Materials for multifunctional balloon catheters with capabilities in cardiac electrophysiological mapping and ablation therapy. *Nat Mater* 10: 316–323, 2011.
20. Lardo AC, McVeigh ER, Jumrussirikul P, Berger RD, Calkins H, Lima J, Halperin HR. Visualization and temporal/spatial characterization of cardiac radiofrequency ablation lesions using magnetic resonance imaging. *Circulation* 102: 698–705, 2000.
21. Li LZ, Zhou R, Xu HN, Moon L, Zhong T, Kim EJ, Qiao H, Reddy R, Leeper D, Chance B, Glickson JD. Quantitative magnetic resonance and optical imaging biomarkers of melanoma metastatic potential. *Proc Natl Acad Sci USA* 106: 6608–6613, 2009.
22. Li LZ, Zhou R, Zhong T, Moon L, Kim EJ, Qiao H, Pickup S, Hendrix MJ, Leeper D, Chance B, Glickson JD. Predicting melanoma metastatic potential by optical and magnetic resonance imaging *Adv. Exp Med Biol* 599: 67–78, 2007.
23. Lo LW, Chen SA. Three-dimensional electroanatomic mapping systems in catheter ablation of atrial fibrillation. *Circ J* 74: 18–23, 2010.
24. Mayevsky A, Chance B. Oxidation-reduction states of NADH in vivo: from animals to clinical use. *Mitochondrion* 7: 330–339, 2007.
25. Menes T, Spivak H. Laparoscopy: searching for the proper insufflation gas. *Surg Endosc* 14: 1050–1056, 2000.
26. Meng X, He G, Zhang J, Han Z, Yu M, Zhang M, Tang Y, Fang L, Zhou X. A comparative study of fibroid ablation rates using radio frequency or high-intensity focused ultrasound. *Cardiovasc Intervent Radiol* 33: 794–799, 2010.
27. Niu G, Scherlag BJ, Lu Z, Ghias M, Zhang Y, Patterson E, Dasari TW, Zacharias S, Lazzara R, Jackman WM, Po SS. An acute experimental model demonstrating 2 different forms of sustained atrial tachyarrhythmias. *Circ Arrhythm Electrophysiol* 2: 384–392, 2009.
28. Perez FJ, Wood MA, Schubert CM. Effects of gap geometry on conduction through discontinuous radiofrequency lesions. *Circulation* 113: 1723–1729, 2006.
29. Roger VL, Go AS, Lloyd-Jones DM, Adams RJ, Berry JD, Brown TM, Carnethon MR, Dai S, de Simone G, Ford ES, Fox CS, Fullerton HJ, Gillespie C, Greenlund KJ, Hailpern SM, Heit JA, Ho PM, Howard VJ, Kissela BM, Kittner SJ, Lackland DT, Lichtman JH, Lisabeth LD, Makuc DM, Marcus GM, Marelli A, Matchar DB, McDermott MM, Meigs JB, Moy CS, Mozaffarian D, Mussolino ME, Nichol G, Paynter NP, Rosamond WD, Sorlie PD, Stafford RS, Turan TN, Turner MB, Wong ND, Wylie-Rosett J, American Heart Association Statistics Committee and Stroke Statistics Subcommittee. Heart disease and stroke statistics—2011 update: a report from the American Heart Association. *Circulation* 123: e18–e209, 2011.
30. Sosa E, Scanavacca M. Epicardial mapping and ablation techniques to control ventricular tachycardia. *J Cardiovasc Electrophysiol* 16: 449–452, 2005.
31. Swartling J, Palsson S, Platonov P, Olsson SB, Andersson-Engels S. Changes in tissue optical properties due to radio-frequency ablation of myocardium. *Med Biol Eng Comput* 41: 403–409, 2003.
32. Swift L, Martell B, Khatri V, Arutunyan A, Sarvazyan N, Kay M. Controlled regional hypoperfusion in Langendorff heart preparations *Physiol Meas* 29: 269–279, 2008.
33. Van Haesendonck C, Sinnaeve A, Willems R, Vandembulcke F, Stroobandt R. Biophysical and electrical aspects of radiofrequency catheter ablation. *Acta Cardiol* 50: 105–115, 1995.
34. Yokoyama K, Nakagawa H, Shah DC, Lambert H, Leo G, Aeby N, Ikeda A, Pitha JV, Sharma T, Lazzara R, Jackman WM. Novel contact force sensor incorporated in irrigated radiofrequency ablation catheter predicts lesion size and incidence of steam pop and thrombus. *Circ Arrhythm Electrophysiol* 1: 354–362, 2008.